Highlighting Thermodynamic Coupling Effects in the Immersion Precipitation Process for Formation of Polymeric Membranes

Krishna, R.

DOI
10.1021/acsomega.9b03609

Publication date
2020

Document Version
Final published version

Published in
ACS Omega

ACS OMEGA

http://pubs.acs.org/journal/acsodf

Article

Highlighting Thermodynamic Coupling Effects in the Immersion Precipitation Process for Formation of Polymeric Membranes

Rajamani Krishna*

Cite This: *ACS Omega* 2020, 5, 2819−2828

Read Online

ACCESS | Metrics & More | Article Recommendations | Supporting Information

ABSTRACT: In the immersion precipitation process for membrane formation, a polymer casting film is placed in contact with a nonsolvent in a coagulation bath; an essential feature of the membrane formation process is the foray into the metastable region of the ternary phase diagram for the nonsolvent/solvent/polymer system. The primary objective of this article is to trace the origins of such forays. The Maxwell−Stefan diffusion formulation is combined with the Flory−Huggins description of phase equilibrium thermodynamics to set up a model for describing the transient equilibration trajectory that is followed in the polymer casting film. Four different systems are analyzed: water/acetone/CA, water/DMF/PVDF, water/NMP/PSF, and water/NMP/PEI (CA = cellulose acetate; PVDF = poly(vinylidene fluoride); PSF = polysulfone; PEI = polyetherimide, DMF = dimethyl formamide; NMP = *N*-methyl-2-pyrrolidone). The analysis shows that diffusional forays are mainly engendered due to thermodynamic coupling effects; such effects are quantified by the set of thermodynamic factors $\Gamma_{ij} = \frac{\phi_i}{\phi_j}\frac{\partial \ln a_i}{\partial \ln \phi_j}$, where a_i, the activity of species i, is dependent on the volume fractions, ϕ_i and ϕ_j, of both nonsolvent (i) and solvent (j). In regions close to phase transitions, the off-diagonal elements $\Gamma_{ij}(i \neq j)$ are often negative and may attain large magnitudes in relation to the diagonal elements Γ_{ii}. Strong thermodynamic coupling effects cause the transient equilibration trajectories to be strongly curvilinear, causing ingress into the metastable region. If thermodynamic coupling effects are ignored, no such ingress occurs. It is also shown that analogous diffusional forays may lead to emulsion formation in partially miscible liquid mixtures.

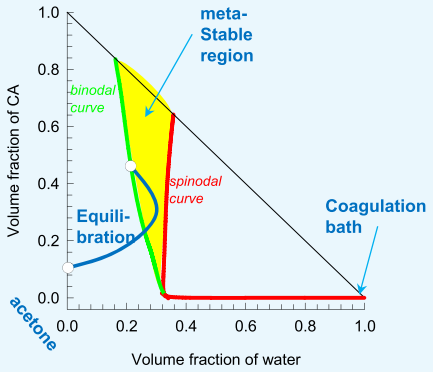

1. INTRODUCTION

The landmark discovery of the asymmetric cellulose acetate (CA) membrane by Loeb and Sourirajan[1] for water desalination has had a significant technological impact on the development of a wide variety of polymer membranes that have several practical applications.[2,3] To set the scene for this article and define its objectives, let us consider the basic principles of the immersion precipitation procedure that was originally used for preparing CA membranes.[3−13] The ternary phase diagram for ternary water/acetone/CA solutions, constructed on the basis of the volume fractions using the Flory−Huggins description of phase equilibrium thermodynamics, is shown in Figure 1. The binodal curve for this ternary mixture defines the limits of phase miscibility; the compositions at the end of a tie-line are in thermodynamic equilibrium requiring equality of component activities, a_i, in the two contiguous fluid phases. The spinodal curve defines the limit of phase stability. Along the spinodal curve, the determinant $|\Gamma| = 0$, where $|\Gamma|$ is a 2×2 dimensional matrix of thermodynamic correction factors with elements defined by

$$\Gamma_{ij} = \frac{\phi_i}{\phi_j}\frac{\partial \ln a_i}{\partial \ln \phi_j};\ i, j = 1, 2 \tag{1}$$

where ϕ_i and ϕ_j denote the volume fractions of water and acetone, respectively.[14,15]

The inset to Figure 1 is a schematic of the immersion precipitation process in which a thin layer of casting film of the acetone/CA mixture, placed on a support layer, is brought into contact with water in a coagulation bath. As illustrated, the transient equilibration trajectory when a 10% solution of CA in acetone is immersed in the coagulation bath is indicated by the solid blue line connecting A and A*. With increasing immersion contact times, the compositions within the polymer casting film will get progressively richer in water and impoverished in acetone.[3,5,6,12,13] Consequently, the equilibration trajectories get progressively closer to the binodal curve. Figure 1 plots the

Received: October 27, 2019
Accepted: January 27, 2020
Published: February 10, 2020

https://dx.doi.org/10.1021/acsomega.9b03609
ACS Omega 2020, 5, 2819−2828

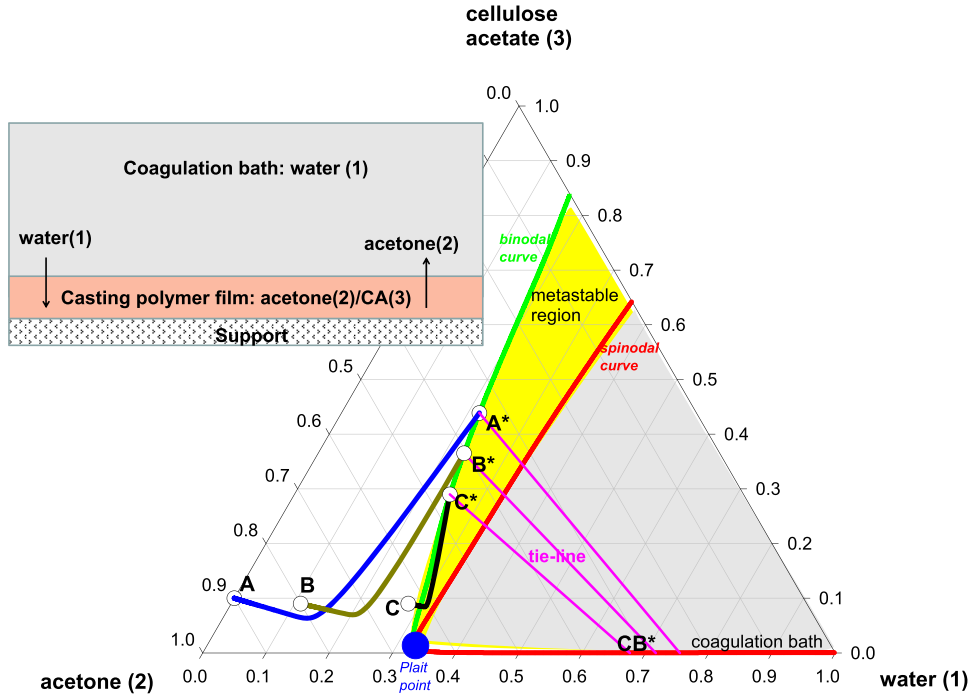

Figure 1. Transient equilibration trajectories A−A*, B−B*, and C−C* during the immersion precipitation process for membrane preparation. These trajectories were determined from simulations using the starting compositions A, B, and C in the polymer casting film. Further calculation details and data inputs are provided in the Supporting Information (SI) accompanying this publication.

progression in the equilibration trajectories A−A*, B−B*, and C−C* with increasing immersion times. All three trajectories are strongly curvilinear. Particularly noteworthy is that the trajectory C−C* has penetrated into the metastable region between the binodal and spinodal curves. This foray into the metastable region causes precipitation of polymer in the casting film. Experimental evidence of such forays is provided by McHugh and Tsay.[16]

The primary objective of this article is to trace the theoretical origins of the diffusional foray into the metastable region as witnessed for the trajectory C−C*. For this purpose, we set up a model to describe the equilibration trajectories by combining the Flory−Huggins description of phase equilibrium with the Maxwell−Stefan formulations for diffusion.[17−21] By detailed analysis of four different systems: water/acetone/CA, water/DMF/PVDF, water/NMP/PSF, and water/NMP/PEI (CA = cellulose acetate; PVDF = poly(vinylidene fluoride); PSF = polysulfone; PEI = polyetherimide; DMF = dimethyl formamide; NMP = *N*-methyl-2-pyrrolidone), we aim to show that the diffusional forays into metastable regions are primarily engendered by thermodynamic coupling effects that are quantified by the off-diagonal elements $\Gamma_{ij}(i \neq j)$. The secondary objective of this article is to demonstrate that the same concepts and modeling approaches are applicable to describe diffusion-induced ingress into metastable regions, resulting in emulsification[22−24] and production of nanospheres and nanoparticles by the exploitation of the "Ouzo effect".[25−27]

2. RESULTS AND DISCUSSIONS

2.1. Maxwell−Stefan Formulation for Diffusion in Ternary Polymer Solutions. For a description of diffusion in ternary nonsolvent (1)/solvent (2)/polymer (m) solutions, it is convenient to use volume fractions, ϕ_i, as composition measures because this facilitates combination with the Flory−Huggins description of phase equilibrium. Let us define the volumetric diffusion fluxes J_i^V, relative to the volume average velocity of the mixture $u^V = \phi_1 u_1 + \phi_2 u_2 + \phi_m u_m$.

$$J_i^V = \phi_i(u_1 - u^V);\ \ i = 1, 2$$
$$J_m^V = \phi_m(u_m - u^V) = -J_1^V - J_2^V \tag{2}$$

The volume fractions are related to the molar concentrations, $\phi_i = c_i \bar{V}_i$, where $\bar{V}_i$ is the partial molar volume of species *i*. The use of u^V as a reference velocity is particularly convenient for polymeric solutions because $\bar{V}_i$ is practically composition independent.

In the Maxwell−Stefan (M−S) formulation, the volumetric diffusion fluxes, J_i^V, expressed in the units $m^3\ m^{-2}\ s^{-1}$, are related to the chemical potential gradients as follows[17,18,20]

$$-\phi_1 \frac{1}{RT}\frac{\partial \mu_1}{\partial z} = \frac{(\phi_2 J_1^V - \phi_1 J_2^V)}{Đ_{12}^V} + \frac{(\phi_m J_1^V - \phi_1 J_m^V)}{Đ_{1m}^V}$$
$$-\phi_2 \frac{1}{RT}\frac{\partial \mu_2}{\partial z} = \frac{(\phi_1 J_2^V - \phi_2 J_1^V)}{Đ_{21}^V} + \frac{(\phi_m J_2^V - \phi_2 J_m^V)}{Đ_{2m}^V} \tag{3}$$

The M−S diffusivities, $Đ_{1m}^V$ and $Đ_{2m}^V$, quantifying interactions ("friction") between species 1 and 2 with the polymer chains are relatable to the self-diffusivities in polymer solutions, for which estimation procedures using the free-volume theory are well established.[28−30] The M−S diffusivities $Đ_{12}^V$ and $Đ_{21}^V$, appearing in the first right members of eq 3, quantify the 1−2 friction. The symmetry constraint demanded by the Onsager reciprocal relations is

$$\frac{Đ_{21}^V}{\bar{V}_1} = \frac{Đ_{12}^V}{\bar{V}_2} \tag{4}$$

The M−S diffusivities $Đ_{12}^V$ and $Đ_{21}^V$ are relatable to the M−S diffusivities in binary nonsolvent/solvent solutions for which reliable estimation procedures are available in the litera-

https://dx.doi.org/10.1021/acsomega.9b03609
ACS Omega 2020, 5, 2819−2828

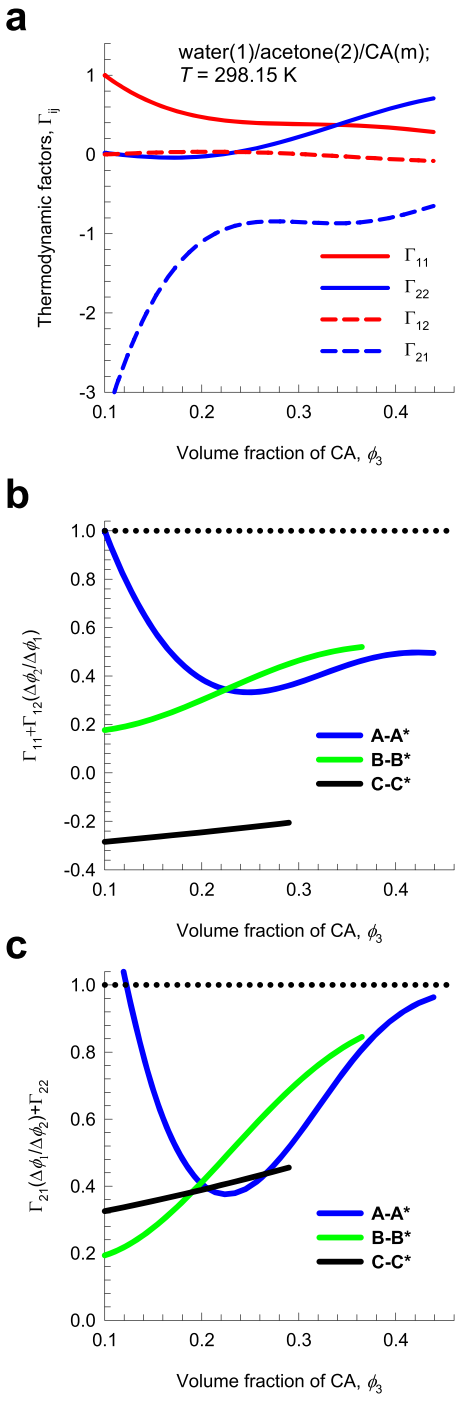

Figure 2. (a) Calculations for the matrix of thermodynamic correction factors, Γ_{ij}. (b, c) Calculations of (b) $\Gamma_{11} + \Gamma_{12}$ $(\Delta\phi_2/\Delta\phi_1)$ and (c) Γ_{21} $(\Delta\phi_1/\Delta\phi_2)$ for volume fractions along a straight line connecting A−A*, B−B*, and C−C* in Figure 1. Further calculation details and data inputs are provided in the Supporting Information accompanying this publication.

ture.[14,15,31,32] Detailed derivations of eq 3, including comparison with the equivalent Bearman friction formulation,[28,30,33,34] along with step-by-step procedures for estimation of the set of M−S diffusivities are provided in the Supporting Information (SI) accompanying this publication.

In view of eq 1, the left members of eq 3 can be expressed in terms of the gradients in the volume fractions

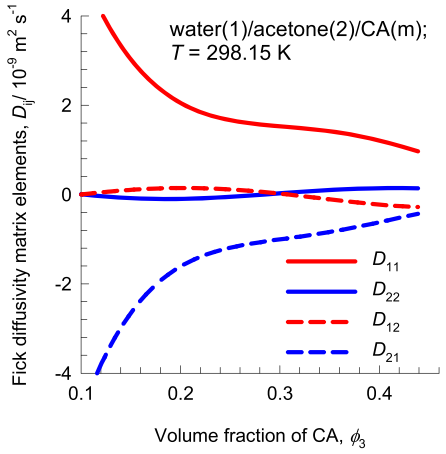

Figure 3. Elements of the Fick diffusivity matrix $[D]$, for water (1)/acetone (2)/CA (m) at T = 298.15 K. Further calculation details and data inputs are provided in the Supporting Information accompanying this publication.

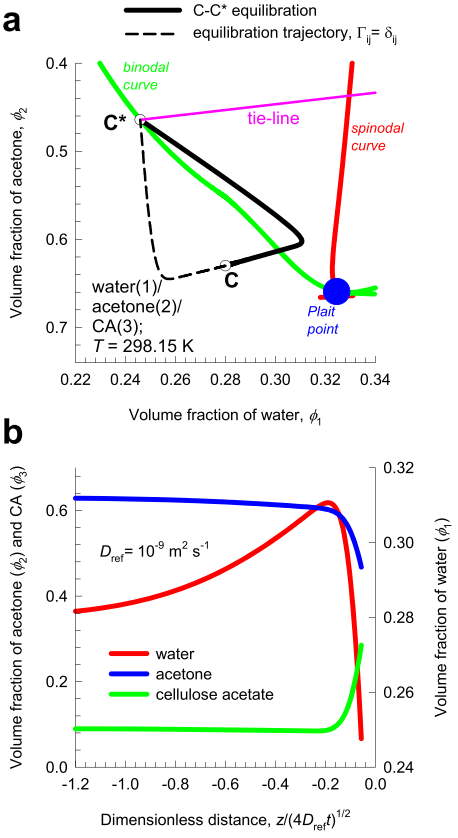

Figure 4. (a) Transient equilibration trajectory C−C* in the water/acetone/casting film. The dashed lines represent simulation results when the simplification $\Gamma_{ij} = \delta_{ij}$, the Kronecker delta, is invoked. (b) Transient volume fraction profiles in the casting solution, as a function of the dimensionless distance coordinate $z/\sqrt{4D_{ref}t}$. Further calculation details and data inputs are provided in the Supporting Information accompanying this publication.

$$\frac{\phi_i}{RT}\frac{\partial \mu_i}{\partial z} = \phi_i \frac{\partial \ln a_i}{\partial z} = \sum_{j=1}^{2} \Gamma_{ij}\frac{\partial \phi_j}{\partial z};\ i, j = 1, 2 \tag{5}$$

For the system water (1)/acetone (2)/CA (3), Figure 2a shows calculations of the four elements Γ_{ij} as a function of the volume

https://dx.doi.org/10.1021/acsomega.9b03609
ACS Omega 2020, 5, 2819−2828

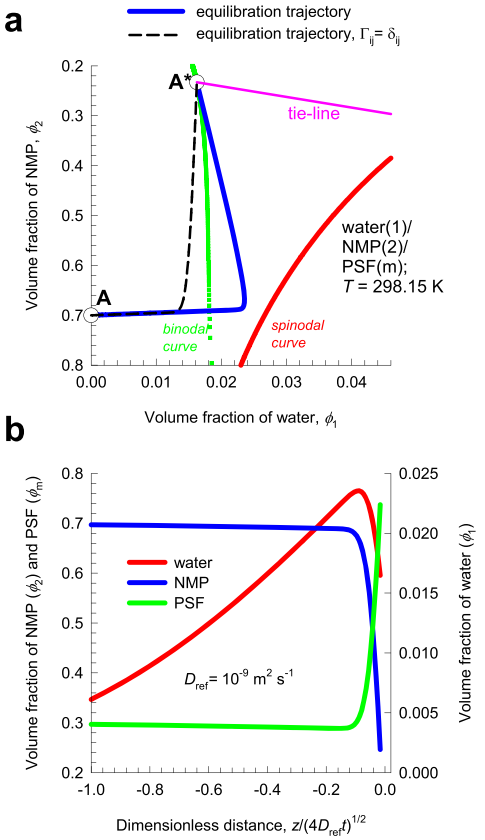

Figure 5. (a) Transient equilibration trajectory A−A* water/NMP/PSF casting film. (b) Transient volume fraction profiles in the casting solution, as a function of the dimensionless distance coordinate $z/\sqrt{4D_{ref}t}$. Further calculation details and data inputs are provided in the Supporting Information accompanying this publication.

fractions of CA that lie on a straight line connecting A ($\phi_{10} = 0.2181$; $\phi_{20} = 0.34308$) with A* ($\phi_{1I} = 0.2181$; $\phi_{2I} = 0.34308$) in Figure 1. Particularly noteworthy are the large negative values of Γ_{21}. Γ_{ij} factors have the effect of influencing the driving forces for the transport of water (1) and acetone (2), into and away from the casting film. Thermodynamic coupling effects on the driving forces for water and acetone transport may be quantified by the factors $\Gamma_{11} + \Gamma_{12}\,(\Delta\phi_2/\Delta\phi_1)$ and $\Gamma_{21}\,(\Delta\phi_1/\Delta\phi_2) + \Gamma_{22}$, where $\Delta\phi_i$ denotes the difference between the interfacial volume fractions, ϕ_{iI}, and those at the start of the equilibration process, ϕ_{i0}

$$\Delta\phi_1 = \phi_{1I} - \phi_{10};\quad \Delta\phi_2 = \phi_{2I} - \phi_{20} \tag{6}$$

These terms are plotted in Figure 2b,c for volume fractions along straight lines connecting A−A*, B−B*, and C−C*. In all three cases, the influence of thermodynamic coupling is to suppress both the driving forces of water and acetone. If thermodynamic coupling effects are ignored by invoking the assumption $\Gamma_{ij} = \delta_{ij}$, the Kronecker delta, both these factors should be unity. Remarkably, we note that for C−C* equilibration, thermodynamic coupling serves not only to reduce the magnitude of the driving force for water transport but also to reverse its sign. The precise consequences of such sign reversals will be elaborated in a later section.

Combining eqs 3 and 5 and casting into matrix notation, we obtain

$$-[\Gamma]\frac{\partial}{\partial z}\begin{pmatrix}\phi_1\\ \phi_2\end{pmatrix} = \begin{bmatrix}\dfrac{\phi_1}{\mathcal{D}_{1m}^{V}} + \dfrac{\phi_2}{\mathcal{D}_{12}^{V}} + \dfrac{\phi_m}{\mathcal{D}_{1m}^{V}} & -\phi_1\left(\dfrac{1}{\mathcal{D}_{12}^{V}} - \dfrac{1}{\mathcal{D}_{1m}^{V}}\right)\\ -\phi_2\left(\dfrac{1}{\mathcal{D}_{21}^{V}} - \dfrac{1}{\mathcal{D}_{2m}^{V}}\right) & \dfrac{\phi_1}{\mathcal{D}_{21}^{V}} + \dfrac{\phi_2}{\mathcal{D}_{2m}^{V}} + \dfrac{\phi_m}{\mathcal{D}_{2m}^{V}}\end{bmatrix}\begin{pmatrix}J_1^{V}\\ J_2^{V}\end{pmatrix} = [B]\begin{pmatrix}J_1^{V}\\ J_2^{V}\end{pmatrix} \tag{7}$$

Premultiplying eq 7 by $[B]^{-1}$, we can explicitly relate the diffusion fluxes to the gradients in the volume fractions

$$\begin{pmatrix}J_1^{V}\\ J_2^{V}\end{pmatrix} = -[D]\frac{\partial}{\partial z}\begin{pmatrix}\phi_1\\ \phi_2\end{pmatrix};\quad [D] = [B]^{-1}[\Gamma] \tag{8}$$

Equation 8 also serves to define the 2 × 2 dimensional square matrix of Fick diffusivities $[D]$, which is a product of two square matrices $[B]^{-1}$ and $[\Gamma]$. Generally speaking, the off-diagonal contributions of each of the two matrices, $[B]^{-1}$ and $[\Gamma]$ are non-negligible; consequently, molecular diffusion in ternary polymer solutions is a strongly coupled process.

Figure 3 shows calculations of the elements of the Fick diffusivity matrix $[D]$ for volume fractions that lie on a straight line connecting A with A* in Figure 1. The variation of the four elements of $[D]$ with the volume fraction of CA shows approximately the same trends as the corresponding elements of the matrix of thermodynamic factors $[\Gamma]$ in Figure 2a. The large negative value of the off-diagonal element D_{21} is largely engendered by the corresponding negative off-diagonal element Γ_{21}.

2.2. Modeling Transient Diffusion in the Immersion Precipitation Process. To meet the objectives of this article, we seek an analytic solution to describe the immersion precipitation transience and essentially follow the model of Tsay and McHugh.[13] The diffusion process is considered to be essentially uni-(z)-directional; the position $z = 0$ corresponds to the position of the interface at the start of the equilibration process. The contiguous immiscible phases, coagulation bath and polymer casting film, are both considered to be semi-infinite. At the position $z = +\infty$, the composition corresponds to that of the bulk coagulation bath that is time-invariant. At the position $z = -\infty$, the composition corresponds to that of the polymer casting film that is in contact with the support layer; this composition is also time-invariant. At any time t, during the immersion precipitation process, we have thermodynamic equilibrium at the interface between the two immiscible phases, at compositions A* and CB*. The volume fractions ϕ_{iI} and ϕ_{1bI} are determined by the thermodynamic equilibrium constraints

$$a_{1I} = a_{1bI};\quad a_{2I} = a_{2bI} \tag{9}$$

The Flory−Huggins (F−H) description of phase equilibrium thermodynamics[17−19,35−37] is used to solve the set of eq 9; calculation details and F−H input parameters for all investigated systems are provided in the SI.

The transient ternary diffusion within the polymer casting film is described by a set of two coupled partial differential equations

https://dx.doi.org/10.1021/acsomega.9b03609
ACS Omega 2020, 5, 2819−2828

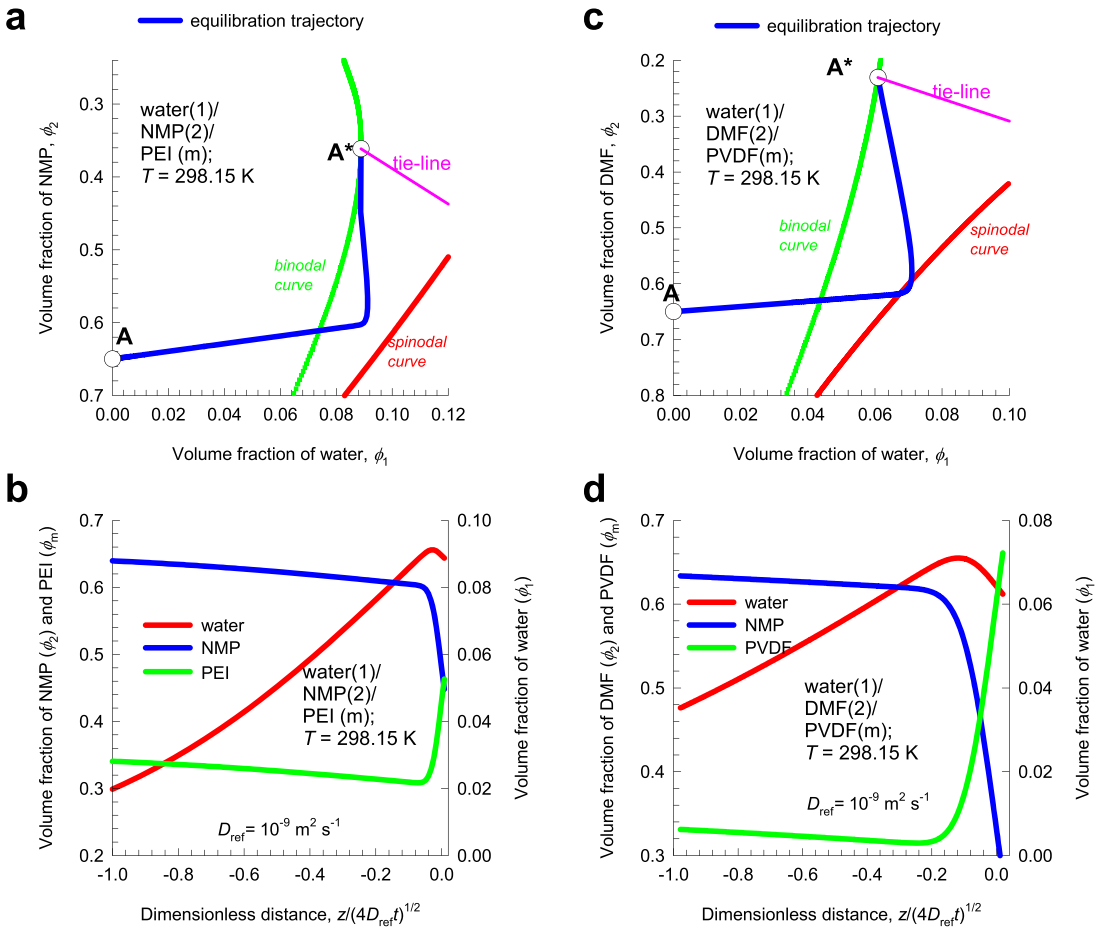

Figure 6. (a, b) Transient equilibration in the water/NMP/PEI casting film. (c, d) Transient equilibration in the water/DMF/PVDF casting film. Further calculation details and data inputs are provided in the Supporting Information accompanying this publication.

$$\frac{\partial\begin{pmatrix}\phi_1\\ \phi_2\end{pmatrix}}{\partial t} = -\frac{\partial\begin{pmatrix}J_1^V\\ J_2^V\end{pmatrix}}{\partial z} \tag{10}$$

Inserting eq 8 for the volumetric fluxes results in

$$\frac{\partial\begin{pmatrix}\phi_1\\ \phi_2\end{pmatrix}}{\partial t} = [D]\frac{\partial^2\begin{pmatrix}\phi_1\\ \phi_2\end{pmatrix}}{\partial z^2} \tag{11}$$

Commonly, the coagulation bath consists of a binary mixture of nonsolvent (1) and solvent (2). As a good approximation, the composition of the coagulation bath may be assumed to be polymer-free. The corresponding relation for the transient diffusion process in the coagulation bath is described by

$$\frac{\partial\phi_{1b}}{\partial t} = D_b\frac{\partial^2\phi_{1b}}{\partial z^2} \tag{12}$$

The subscript b in eq 12 refers to the coagulation bath, and D_b represents the Fick diffusivity in the binary solution in the bath.

The initial conditions for eqs 11 and 12 are

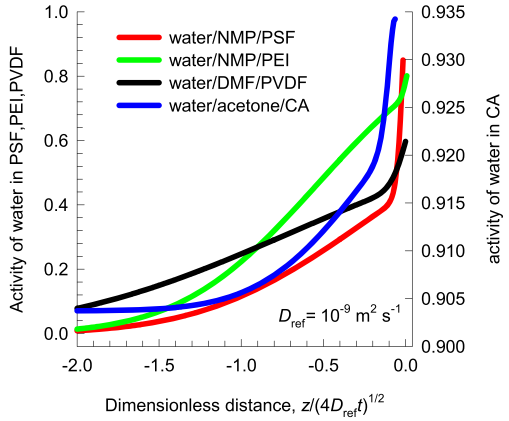

Figure 7. Transient profiles of water activity in the casting solution for water/acetone/CA, water/NMP/PSF, water/NMP/PEI, and water/DMF/PVDF plotted as a function of the dimensionless distance coordinate $z/\sqrt{4D_{ref}t}$.

$$z \geq 0,\ t = 0, \quad \begin{pmatrix}\phi_1(z,0)\\ \phi_2(z,0)\end{pmatrix} = \begin{pmatrix}\phi_{10}\\ \phi_{20}\end{pmatrix}$$

$$z \leq 0,\ t = 0, \quad \phi_{1b}(z,0) = \phi_{1b0} \tag{13}$$

where ϕ_{i0} and ϕ_{1b0} are the initial compositions of the polymer casting film and bath, respectively.

https://dx.doi.org/10.1021/acsomega.9b03609
ACS Omega 2020, 5, 2819−2828

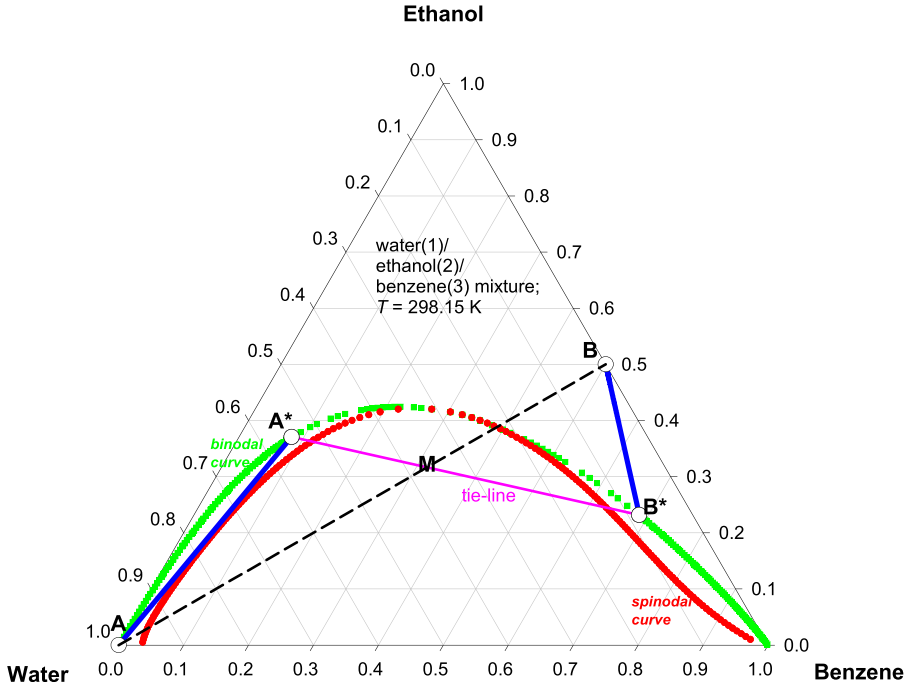

Figure 8. Transient equilibration trajectories A−A* and B−B* for the water/ethanol/benzene mixture at 298 K, demonstrating foray into the metastable region in the water-rich region of the phase diagram. The solid blue lines represent the trajectories calculated using the Ruschak−Miller model. Further calculation details and data inputs are provided in the Supporting Information accompanying this publication.

The boundary conditions are

$$z = -\infty, \quad t \geq 0, \quad \begin{pmatrix} \phi_1(-\infty, t) \\ \phi_2(-\infty, t) \end{pmatrix} = \begin{pmatrix} \phi_{10} \\ \phi_{20} \end{pmatrix}$$

$$z = +\infty, \quad t \geq 0, \quad \phi_{1b}(+\infty, t) = \phi_{1b0} \tag{14}$$

An analytic solution for the transient volume fractions in the bath is obtained if the Fick diffusivity D_b is assumed to be composition independent[13,38]

$$\phi_{1b}(z, t) = \phi_{1b0} + \frac{\text{erfc}\left(\frac{z}{\sqrt{4D_b t}}\right)}{\text{erfc}\left(\frac{r}{\sqrt{4D_b}}\right)}(\phi_{1bI} - \phi_{1b0}) \tag{15}$$

The corresponding analytic expression for the volume fractions in the polymer casting film is also derivable if the Fick diffusivity matrix $[D] = [B]^{-1}[\Gamma]$ is also assumed to be composition independent; see Taylor and Krishna.[31] In all of the calculations presented in this article, the Fick $[D]$ is evaluated at the average volume fractions $\frac{1}{2}\begin{pmatrix} \phi_{10} + \phi_{1I} \\ \phi_{20} + \phi_{2I} \end{pmatrix}$; this linearization procedure has been established to yield results of good accuracy.[18] The transient volume fractions in the polymer film can be written as 2 × 2 dimensional matrix generalization of eq 15; see Taylor and Krishna[31] for further theoretical background on matrix generalization procedures

$$\begin{pmatrix} \phi_1(z, t) \\ \phi_2(z, t) \end{pmatrix} = \begin{pmatrix} \phi_{10} \\ \phi_{20} \end{pmatrix} + \left[\text{erfc}\left(-\frac{z}{\sqrt{4t}}[D]^{-1/2}\right)\right] \left[\text{erfc}\left(-\frac{r}{2}[D]^{-1/2}\right)\right]^{-1} \begin{pmatrix} \phi_{1I} - \phi_{10} \\ \phi_{2I} - \phi_{20} \end{pmatrix} \tag{16}$$

Due to interchange of nonsolvent and solvent between the polymer casting film and the bath, the position of the interface, $\varepsilon(t) = r\sqrt{t}$, will shift with time

$$\begin{pmatrix} \phi_1(\varepsilon(t), t) \\ \phi_2(\varepsilon(t), t) \end{pmatrix} = \begin{pmatrix} \phi_{1I} \\ \phi_{2I} \end{pmatrix}; \quad \phi_{3I} = 1 - \phi_{1I} - \phi_{2I}$$

$$\phi_{1b}(\varepsilon(t), t) = \phi_{1bI} = 1 - \phi_{2bI} \tag{17}$$

In eq 17, $\varepsilon(t) = r\sqrt{t}$ is the position of the moving interface, and r is a constant with units of m $s^{-1/2}$, which is determinable from the continuity of component fluxes at either side of the moving interface

$$J_i^V|_{z=\varepsilon(t)} - J_{ib}^V|_{z=\varepsilon(t)} = (\phi_{iI} - \phi_{ibI})\frac{d\varepsilon(t)}{dt} = (\phi_{iI} - \phi_{ibI})\frac{r}{2\sqrt{t}}; \quad i = 1, 2 \tag{18}$$

The simultaneous solution of the set of four nonlinear eqs 9 and 18 allows calculation of the interfacial compositions ϕ_{1I}, ϕ_{2I}, ϕ_{1bI}, and r.

2.3. Simulations of Four Immersion Precipitation Processes. First, we investigate in detail the C−C* equilibration trajectory followed in the water/acetone/CA casting film when the initial volume fractions in the casting film are chosen as $\phi_{10} = 0.28$; $\phi_{20} = 0.63$; $\phi_{1b0} = 0.75$; and $\phi_{2b0} = 0.25$; corresponding to the position C indicated in Figure 1. The simultaneous solution of the equations describing thermodynamic equilibrium at the interface (eq 9) and the flux continuity relations (eq 18) results in the interfacial volume fractions $\phi_{1I} = 0.24596$; $\phi_{2I} = 0.46422$; and $\phi_{1bI} = 0.6753$; these correspond to C* and CB*. The value of $r = -3.46302 \times 10^{-6}$ is negative because of the shrinkage of the polymer casting film due to the impoverishment of acetone. Evaluated at the arithmetic average volume fractions between the initial and final equilibrated

https://dx.doi.org/10.1021/acsomega.9b03609
ACS Omega 2020, 5, 2819−2828

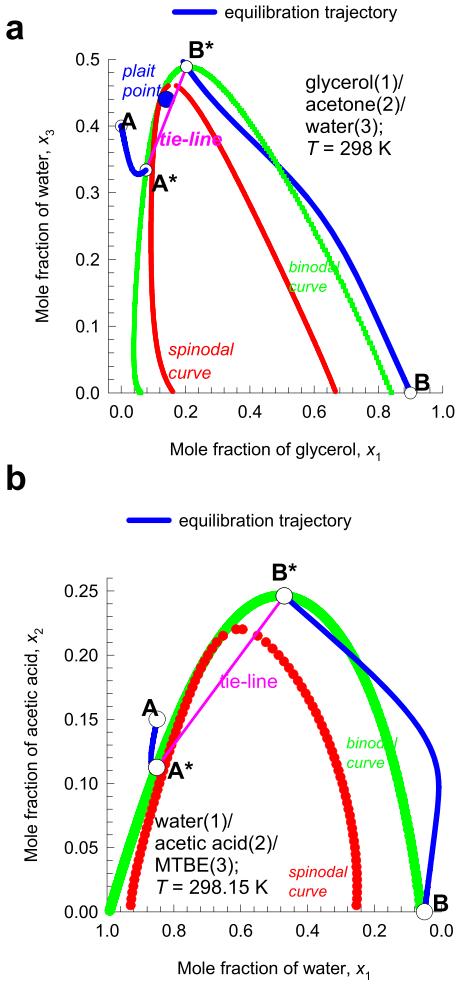

Figure 9. (a) Transient equilibration trajectories for the glycerol (1)/acetone (2)/water (3) mixture at 298 K, demonstrating foray into the meta-region in the glycerol-rich phase. (b) Transient equilibration trajectories for the system water (1)/acetic acid (2)/MTBE (3) at 298 K, demonstrating forays into the metastable region in the MTBE-rich phase. Further calculation details and data inputs are provided in the Supporting Information accompanying this publication.

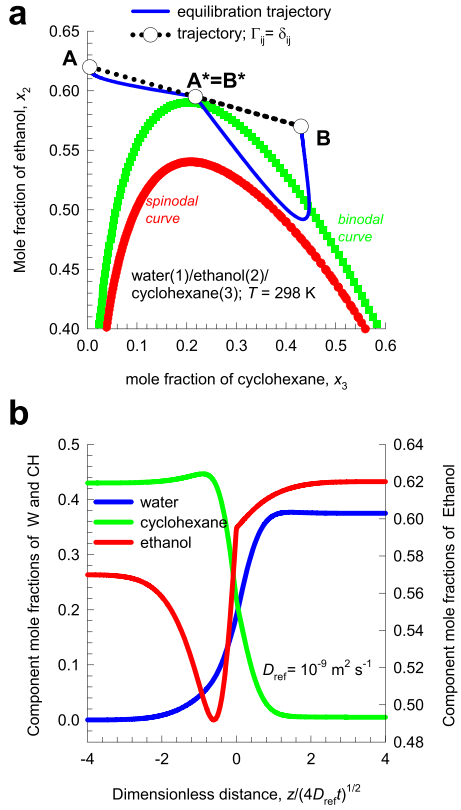

Figure 10. (a) Trajectories followed during transient equilibration of homogenous mixtures of two different compositions A and B for the system water (1)/ethanol (2)/cyclohexane (3) at 298 K. (b) Transient composition profiles plotted as a function of the dimensionless distance coordinate $z/\sqrt{4D_{ref}t}$. Further calculation details and data inputs are provided in the Supporting Information accompanying this publication.

compositions, $\frac{1}{2}\begin{pmatrix}\phi_{10}+\phi_{1I}\\ \phi_{2I}+\phi_{2I}\end{pmatrix}$, the elements of the matrix of thermodynamic factors, and the Fick diffusivity matrix are: $[\Gamma] = \begin{bmatrix}0.15393 & -0.08279\\ -0.53829 & 0.49255\end{bmatrix}$ and $[D] = \begin{bmatrix}0.46829 & -0.25204\\ -0.36327 & 0.21014\end{bmatrix} \times 10^{-9}$ m^2 s^{-1}. Noteworthy are the large negative values of both off-diagonal elements Γ_{12} and Γ_{21}. Both off-diagonal elements D_{12} and D_{21} are also negative, primarily because of the corresponding negative values of Γ_{12} and Γ_{21}.

The equilibration trajectory calculated using eq 16 is plotted in Figure 4a composition space; we note that the C−C* is strongly curvilinear and has penetrated into the metastable region.

The volume fractions of the three components are plotted in Figure 4b as a function of the dimensionless distance coordinate $z/\sqrt{4D_{ref}t}$ in the casting film, where we take the value of the reference diffusivity $D_{ref} = 1 \times 10^{-9}$ m^2 s^{-1}. There is a significantly higher volume fraction of the polymer near the surface of the casting film, $z \approx 0$. This implies that the polymer distributes asymmetrically across the membrane thickness, resulting in an asymmetric polymer membrane. Also noteworthy is that the volume fraction of water shows a pronounced overshoot at $z/\sqrt{4D_{ref}t} \approx -0.2$; this overshoot signifies uphill diffusion.[14,32,39] The overshoot in water is a direct result of the influence of thermodynamic coupling on the driving force of water, causing the effective driving force to undergo sign reversal, as witnessed in Figure 2b.

To delineate the influence of thermodynamic coupling, we repeated the simulations by invoking the assumption $\Gamma_{ij} = \delta_{ij}$ and calculating the Fick matrix using $[D] = [B]^{-1}$; this results in C−C* trajectory indicated by the dashed line in Figure 4a. No ingress into the metastable region is experienced, and the trajectory tends to veer away from the binodal curve in its approach to C*. The inescapable conclusion is that the influence of the thermodynamic correction factors is to draw the trajectories into the metastable region, leading eventually to polymer precipitation.

Next, we analyze the transient equilibration trajectory followed in the ternary water/NMP/PSF solutions in which the initial volume fractions in the polymer casting film and coagulation bath are chosen as $\phi_{10} = 0$; $\phi_{20} = 0.7$; $\phi_{1b0} = 0.3$; $\phi_{2b0} = 0.7$, corresponding to the position A indicated in Figure 5a. The simultaneous solution of the equations describing thermodynamic equilibrium at the interface (eq 9) and the flux continuity relations (eq 18) results in the interfacial volume fractions $\phi_{1I} = 0.01623$; $\phi_{2I} = 0.23293$; and $\phi_{1bI} = 0.25625$. Both

https://dx.doi.org/10.1021/acsomega.9b03609
ACS Omega 2020, 5, 2819−2828

the off-diagonal elements of $[\Gamma] = \begin{bmatrix} 0.93085 & -0.01965 \\ -5.36896 & 0.46328 \end{bmatrix}$ and $[D] = \begin{bmatrix} 1.39456 & -0.02938 \\ -0.6735 & 0.01775 \end{bmatrix} \times 10^{-9}$ m^2 s^{-1} are negative. The strong coupling effects cause the A−A* equilibration trajectory to exhibit a foray into the metastable region. The dashed line in Figure 5a represents the trajectory followed by invoking the assumption $\Gamma_{ij} = \delta_{ij}$ and ignoring thermodynamic correction factors; in this scenario, the A−A* does not cross the binodal curve.

The volume fractions of the three components are plotted in Figure 5a as a function of the dimensionless distance coordinate $z/\sqrt{4D_{ref}t}$ in the casting film. The polymer composition is significantly higher near the surface of the casting film, $z \approx 0$, resulting eventually in an asymmetric PSF membrane. The transient overshoot of water signifies uphill transport.

The analyses of the A−A* equilibration trajectories for water/NMP/PEI and water/DMF/PVDF solutions proceed along precisely analogous lines; the results are summarized in Figure 6a−d. Incursions into the metastable regions, induced by off-diagonal elements $\Gamma_{ij} (i \neq j)$, are experienced in both cases. Uphill diffusion causes overshoots in water compositions near the surface of the casting films, and the congregation of PEI and PVDF polymers near the surface of the casting film, $z \approx 0$, is also evident in Figure 6b,d.

The phenomena of uphill diffusion resulting in transient overshoots of water experienced in the four examples above are, however, not in violation of the second law of thermodynamics.[32,39] As verification, the corresponding transient profiles of the activity of water are plotted in Figure 7; in all four cases, the variation of activity along the dimensionless distance is monotonic. Put another way, water transport is down the activity hill.

2.4. Emulsion Formation in Partially Miscible Liquid/Liquid Mixtures. We now demonstrate analogies between the immersion precipitation process with emulsion formation. According to Miller,[22] "If the two bulk liquids are not initially at equilibrium, it is conceivable that dynamic processes such as diffusion could produce emulsification when the two liquids are brought into contact without stirring." The necessary conditions for spontaneous emulsification are derived by Ruschak and Miller[23] in terms of diffusion equilibration composition trajectories that must necessarily enter the metastable regions. These authors adopted the Fickian formulation in which the diffusion flux of each species i is considered to be linearly dependent on its own composition gradient, with the Fickian diffusivities of each component equal to one another.

As illustrated, Figure 8 shows the phase diagram for the partially miscible water (1)/ethanol (2)/benzene (3) mixtures at 298 K. Bringing pure water (indicated by A) in contact with a 50:50 ethanol/benzene mixture (indicated by B) results in a mixture composition (indicated by M) that ends up in the two-phase region of the phase diagram. This mixture will separate into two liquid phases of compositions A* and B* that lie on the binodal curve at either end of the tie-line. The phase A will equilibrate to the composition A*, while phase B will equilibrate to B*. Using the model of Ruschak and Miller,[23] wherein all of the component diffusivities in the ternary mixture are equal to one another, the diffusion equilibration trajectories A−A* and B−B* will both be straight lines in ternary composition space. We note that the A−A* trajectory lies in the metastable region between the binodal and spinodal curves. This foray into the metastable region is a necessary condition for emulsification to occur. Vitale and Katz[27] have coined the generic term Ouzo effect to describe such a process of creating metastable liquid−liquid dispersions. Since no input of mechanical energy is involved, this offers an energy-efficient method of producing nanospheres and nanoparticles.[25]

The Ruschak−Miller model is overly simplistic because the linear equilibration trajectories are only realized if the thermodynamic correction factors are ignored, $\Gamma_{ij} = \delta_{ij}$, and the Fick diffusivity matrix $[D]$, in either contiguous fluid phase, degenerates to a scalar diffusivity times the identity matrix.[14,15] Detailed analysis of the published experimental data on diffusivities in several partially miscible ternary liquid mixtures reveals that the interdiffusion process is strongly coupled due to thermodynamic correction factors close to regions of phase transitions, and the off-diagonal elements of the Fick diffusivity matrix $[D]$ exert significant influences on the equilibration trajectories.[14,15,32,39]

The model for the immersion precipitation process is amenable to the straight-forward extension to cater for interdiffusion between two partially miscible liquid phases (A, B), with two different Fick diffusivity matrices $[D_A]$ and $[D_B]$; the detailed derivations are available in the SI.

Figure 9a shows the simulation results for A−A* and B−B* equilibration trajectories for glycerol/acetone/water mixtures; both trajectories are both strongly curvilinear in composition space; in the glycerol-rich phase, the B−B* exhibits a foray into the metastable region with the potential for emulsification. Similarly, for water/acetic acid/MTBE mixtures, the ingress of B−B* into the metastable region (see Figure 9b) in the MTBE-rich phase may result in emulsion formation. Analogous results are obtained for water/chloroform/acetic acid, water/acetone/ethyl-acetate, water/ethanol/ethyl-acetate, and water/acetic acid/1-hexanol mixtures; see simulation results in Figures S24, S25, S27, and S29. It is noteworthy that the Ruschak−Miller model with straight-line equilibration would also have anticipated the possibilities of emulsification for all of the aforementioned six mixtures.

We now demonstrate scenarios in which forays into metastable regions can occur under conditions that are not anticipated using the model of Ruschak and Miller.[23] For water (1)/ethanol (2)/cyclohexane (3) mixtures, we choose the set of starting compositions for the ethanol-rich phase (A) and cyclohexane-rich phase (B) as $x_{1A0} = 0.375$; $x_{2A0} = 0.62$; $x_{1B0} = 0$; $x_{2B0} = 0.57$; see Figure 10a. The composition of the A−B mixture, A* = B* = $x_{1I} = 0.1875$; $x_{2I} = 0.595$, lies in the homogeneous single-phase region, but close to the binodal curve. According to the Ruschak−Miller analysis, no entry into the metastable regions is possible. Calculations of the A−A* and B−B* trajectories with reliable estimates of the Maxwell−Stefan diffusivities, along with proper accounting of thermodynamic correction factors (using the NRTL equation for phase equilibrium), lead to curvilinear trajectories. The B−B* penetrates the metastable zone in the cyclohexane-rich phase. The composition profiles of the three components are plotted in Figure 10b as a function of the dimensionless distance coordinate $z/\sqrt{4D_{ref}t}$. We note that ethanol experiences a pronounced undershoot during the transient equilibration process. Concomitantly, cyclohexane displays a slight overshoot. The overshoot/undershoot phenomena, along with the entry into the metastable zone, are engendered by the significant off-diagonal elements of $[\Gamma_B] = \begin{bmatrix} 0.59141 & -0.19602 \\ -0.70702 & 0.3644 \end{bmatrix}$ in the cyclohexane-rich phase. Indeed, if thermodynamic coupling

https://dx.doi.org/10.1021/acsomega.9b03609
ACS Omega 2020, 5, 2819−2828

effects are completely ignored by invoking the assumption $\Gamma_{ij} = \delta_{ij}$, the equilibration trajectory (shown by the dotted line in Figure 10a) shows no entry into the metastable region.

Analyses of transient equilibration in glycerol/acetone/water, water/acetone/ethyl-acetate, water/acetic acid/1-hexanol, and water/acrylonitrile/toluene mixtures yield results that are precisely analogous to those in Figure 10; see Figures S23, S26, S29, S32, and S33. In all cases, thermodynamic coupling induces entry into metastable zones, while the Ruschak–Miller model calculations do not anticipate such incursions.

The crystal formation and growth as a consequence of diffusional foray into supersaturated regions is also a consequence of thermodynamic coupling.[32,40]

3. CONCLUSIONS

For partially miscible ternary fluid mixtures, diffusivities in regions close to phase transitions are strongly influenced by phase equilibrium thermodynamics. These influences are quantified by thermodynamic correction factors Γ_{ij}, whose off-diagonal elements Γ_{12} and Γ_{21} are often significantly large in relation to the Γ_{11} and Γ_{22}. Consequently, interphase diffusion is a strongly coupled process that results in strongly curvilinear equilibration trajectories during transient equilibration. Such trajectories often signify uphill diffusion phenomena, and cause forays into the metastable regions, lying between the binodal and spinodal curves. Such forays are essential in the immersion precipitation process for the preparation of CA, PSF, PEI, and PVDF membranes, with asymmetry in the polymer distribution along the thickness. In all cases, if the off-diagonal elements Γ_{12} and Γ_{21} are set to zero, no polymer precipitation is realized. The transient development of volume fractions of water in the polymer casting film exhibits overshoots in all of the four cases; such overshoots are signatures of uphill diffusion. The theoretical model developed in this work should provide guidelines to the polymer chemist for choosing a set of operating conditions, and mixture compositions in the casting film and coagulation bath to prepare asymmetric polymeric membranes.

The exploitation of the Ouzo effect for the formation of metastable emulsions in liquid/liquid mixtures is also crucially dependent on thermodynamic coupling effects.

■ ASSOCIATED CONTENT

Supporting Information

The Supporting Information is available free of charge at https://pubs.acs.org/doi/10.1021/acsomega.9b03609.

(1) Detailed development of the Maxwell–Stefan (M–S) diffusion equations for multicomponent fluid mixtures; (2) comparison of the M–S formulation with the Bearman friction formulation; (3) procedures for estimation of the M–S diffusivities; (4) description of phase equilibrium using the Flory–Huggins relations; (5) development of the analytic model to describe equilibration in the immersion precipitation process; (6) detailed development of the model to describe emulsification in ternary fluid mixtures, and (7) data inputs and simulation details for all investigated mixtures (PDF)

■ AUTHOR INFORMATION

Corresponding Author

Rajamani Krishna − *Van 't Hoff Institute for Molecular Sciences, University of Amsterdam 1098 XH Amsterdam, The Netherlands;* orcid.org/0000-0002-4784-8530; Email: r.krishna@contact.uva.nl

Complete contact information is available at: https://pubs.acs.org/10.1021/acsomega.9b03609

Notes

The author declares no competing financial interest.

■ ACKNOWLEDGMENTS

The author acknowledges the contribution of Dr J. M. van Baten for providing codes for calculation of phase equilibria.

■ NOMENCLATURE

Latin Alphabet

a_i	component activity, dimensionless
$[B]$	matrix of inverse M–S coefficients, m^{-2} s
c_i	molar concentration of species i, mol m^{-3}
$Đ_{ij}^{V}$	M–S diffusivity for binary pair i–j, m^2 s^{-1}
$[D]$	Fick diffusivity matrix, m^2 s^{-1}
$[I]$	identity matrix, dimensionless
J_i^{V}	volumetric diffusion fluxes with respect to u^{V}, m^3 m^{-2} s^{-1}
n	number of species in the mixture, dimensionless
R	gas constant, 8.314 J mol^{-1} K^{-1}
t	time, s
T	absolute temperature, K
x_i	mole fraction of component i in bulk fluid phase, dimensionless
u^{V}	volume average mixture velocity, m s^{-1}
$\overline{V}_i$	partial molar volume of species i, m^3 mol^{-1}
z	direction coordinate, m

■ GREEK ALPHABET

γ_i	activity coefficient of component i, dimensionless
δ_{ij}	Kronecker delta, dimensionless
$\varepsilon(t)$	position of moving boundary, m
Γ_{ij}	thermodynamic correction factors, dimensionless
μ_i	molar chemical potential, J mol^{-1}
ϕ_i	volume fraction of species i, dimensionless

■ SUBSCRIPT

i	referring to component i
I	referring to the interface
m	refers to polymer
n	referring to component n
t	referring to the total mixture

■ SUPERSCRIPT

V volume average reference velocity frame

■ MATRIX NOTATION

()	column matrix
[]	square matrix

■ REFERENCES

(1) Loeb, S.; Sourirajan, S. Sea Water Demineralization by Means of an Osmotic Membrane. In *Saline Water Conversion II*; Gould, R. F., Ed.; Advances in Chemistry Series; American Chemical Society, 1963; Chapter 9, pp 117–132.

(2) Ulbricht, M. Advanced Functional Polymer Membranes. *Polymer* **2006**, *47*, 2217–2262.

(3) van de Witte, P.; Dijkstra, P. J.; van den Berg, J. W. A.; Feijen, J. Phase separation processes in polymer solutions in relation to membrane formation. *J. Membr. Sci.* **1996**, *117*, 1−31.
(4) van den Berg, G. B.; Smolders, C. A. Diffusional phenomena in membrane separation processes. *J. Membr. Sci.* **1992**, *73*, 103−118.
(5) Reuvers, A. J.; Smolders, C. A. Formation of membranes by means of immersion precipitation Part II. The mechanism of formation of membranes prepared from the system cellulose acetate - acetone - water. *J. Membr. Sci.* **1987**, *34*, 67−86.
(6) Reuvers, A. J.; van den Berg, J. W. A.; Smolders, C. A. Formation of membranes by means of immersion precipitation Part II. The mechanism of formation of membranes prepared from the system cellulose acetate - acetone - water. *J. Membr. Sci.* **1987**, *34*, 45−65.
(7) Radovanovic, P.; Thiel, S. W.; Hwang, S.-T. Formation of asymmetric polysulfone membranes by immersion precipitation. Part I. Modelling mass transport during gelation. *J. Membr. Sci.* **1992**, *65*, 213−229.
(8) Radovanovic, P.; Thiel, S. W.; Hwang, S.-T. Formation of asymmetric polysulfone membranes by immersion precipitation. Part II. The effects of casting solution and gelation bath compositions on membrane structure and skin formation. *J. Membr. Sci.* **1992**, *65*, 231−246.
(9) Strathmann, H.; Kock, K. The Formation Mechanism of Phase Inversion Membranes. *Desalination* **1977**, *21*, 2411−2255.
(10) Guillen, G. R.; Yinjin Pan, Y.; Li, M.; Hoek, E. V. Preparation and Characterization of Membranes Formed by Nonsolvent Induced Phase Separation: A Review. *Ind. Eng. Chem. Res.* **2011**, *50*, 3798−3817.
(11) Wang, D.-M.; Lai, J.-Y. Recent advances in preparation and morphology control of polymeric membranes formed by nonsolvent induced phase separation. *Curr. Opin. Chem. Eng.* **2013**, *2*, 229−237.
(12) Tsay, C. S.; McHugh, A. J. Mass Transfer Modeling of Asymmetric Membrane Formation by Phase Inversion. *J. Polym. Sci., Part B: Polym. Phys.* **1990**, *28*, 1327−1365.
(13) Tsay, C. S.; McHugh, A. J. An Improved Numerical Algorithm for Ternary Diffusion with a Moving Interface. *Chem. Eng. Sci.* **1991**, *46*, 1179−1187.
(14) Krishna, R. Serpentine Diffusion Trajectories and the Ouzo Effect in Partially Miscible Ternary Liquid Mixtures. *Phys. Chem. Chem. Phys.* **2015**, *17*, 27428−27436.
(15) Krishna, R. Highlighting Diffusional Coupling Effects in Ternary Liquid Extraction and Comparisons with Distillation. *Ind. Eng. Chem. Res.* **2016**, *55*, 1053−1063.
(16) McHugh, A. J.; Tsay, C. S. Dynamics of the Phase Inversion Process. *J. Appl. Polym. Sci.* **1992**, *46*, 2011−2021.
(17) Krishna, R. Describing Mixture Permeation across Polymeric Membranes by a Combination of Maxwell-Stefan and Flory-Huggins Models. *Polymer* **2016**, *103*, 124−131.
(18) Krishna, R. Using the Maxwell-Stefan formulation for Highlighting the Influence of Interspecies (1-2) Friction on Binary Mixture Permeation across Microporous and Polymeric Membranes. *J. Membr. Sci.* **2017**, *540*, 261−276.
(19) Krishna, R. Highlighting Thermodynamic Coupling Effects in Alcohol/Water Pervaporation across Polymeric Membranes. *ACS Omega* **2019**, *4*, 15255−15264.
(20) Ribeiro, C. P.; Freeman, B. D.; Paul, D. R. Modeling of Multicomponent Mass Transfer across Polymer Films using a Thermodynamically Consistent Formulation of the Maxwell-Stefan Equations in terms of Volume Fractions. *Polymer* **2011**, *52*, 3970−3983.
(21) Fornasiero, F.; Prausnitz, J. M.; Radke, C. J. Multicomponent Diffusion in Highly Asymmetric Systems. An Extended Maxwell-Stefan Model for Starkly Different-Sized, Segment-Accessible Chain Molecules. *Macromolecules* **2005**, *38*, 1364−1370.
(22) Miller, C. A. Spontaneous Emulsification Produced by Diffusion - A Review. *Colloids Surf.* **1988**, *29*, 89−102.
(23) Ruschak, K. J.; Miller, C. A. Spontaneous Emulsification in Ternary Systems with Muss Transfer. *Ind. Eng. Chem. Fundam.* **1972**, *11*, 534−540.
(24) Jackson, R. Diffusion in Ternary Mixtures with and without Phase Boundaries. *Ind. Eng. Chem. Fundam.* **1977**, *16*, 304−306.
(25) Ganachaud, F.; Katz, J. L. Nanoparticles and Nanocapsules Created Using the Ouzo Effect: Spontaneous Emulsification as an Alternative to Ultrasonic and High-Shear Devices. *ChemPhysChem* **2005**, *6*, 209−216.
(26) Sitnikova, N. L.; Sprik, R.; Wegdam, G.; Eiser, E. Spontaneously Formed trans-Anethol/Water/Alcohol Emulsions: Mechanism of Formation and Stability. *Langmuir* **2005**, *21*, 7083−7089.
(27) Vitale, S. A.; Katz, J. L. Liquid Droplet Dispersions Formed by Homogeneous Liquid-Liquid Nucleation: "The Ouzo Effect". *Langmuir* **2003**, *19*, 4105−4110.
(28) Alsoy, S.; Duda, J. L. Modeling of Multicomponent Drying of Polymer Films. *AIChE J.* **1999**, *45*, 896−905.
(29) Zielinski, J. M.; Hanley, B. F. Practical Friction-Based Approach to Modeling Multicomponent Diffusion. *AIChE J.* **1999**, *45*, 1−12.
(30) Price, P. E.; Romdhane, I. H. Multicomponent Diffusion Theory and Its Applications to Polymer-Solvent Systems. *AIChE J.* **2003**, *49*, 309−322.
(31) Taylor, R.; Krishna, R. *Multicomponent Mass Transfer*; John Wiley & Sons: New York, 1993.
(32) Krishna, R. Diffusing Uphill with James Clerk Maxwell and Josef Stefan. *Chem. Eng. Sci.* **2019**, *195*, 851−880.
(33) Bearman, R. J. On the Molecular Basis of some Current Theories of Diffusion. *J. Phys. Chem. A.* **1961**, *65*, 1961−1968.
(34) Vrentas, J. S.; Duda, J. L. Molecular diffusion in polymer solutions. *AIChE J.* **1979**, *25*, 1−24.
(35) Mulder, M. H. V.; Franken, A. C. M.; Smolders, C. A. Preferential Sorpton versus Preferential Permeability in Pervaporation. *J. Membr. Sci.* **1985**, *22*, 155−178.
(36) Yang, T.-H.; Lue, S. J. Modeling Sorption Behavior for Ethanol/Water Mixtures in a Cross-linked Polydimethylsiloxane Membrane Using the Flory-Huggins Equation. *J. Macromol. Sci., Part B: Phys.* **2013**, *52*, 1009−1029.
(37) Varady, M. J.; Pearl, T. P.; Stevenson, S. M.; Mantooth, B. A. Decontamination of VX from Silicone: Characterization of Multicomponent Diffusion Effects. *Ind. Eng. Chem. Res.* **2016**, *55*, 3139−3149.
(38) Crank, J. *The Mathematics of Diffusion*, 2nd ed.; Clarendon Press: Oxford, 1975.
(39) Krishna, R. Uphill Diffusion in Multicomponent Mixtures. *Chem. Soc. Rev.* **2015**, *44*, 2812−2836.
(40) Myerson, A. S.; Lo, P. Y. Cluster Formation and Diffusion in Supersaturated Binary and Ternary Acid Solutions. *J. Cryst. Growth* **1991**, *110*, 26−33.

https://dx.doi.org/10.1021/acsomega.9b03609
ACS Omega 2020, 5, 2819−2828